# Electron-Beam-Induced Damage in Self-Assembled Monolayers

**Kannan Seshadri,[†] Karl Froyd, Atul N. Parikh,[‡] and David L. Allara*[,†,‡]**

*Departments of Chemistry and Materials Science, Pennsylvania State University, University Park, Pennsylvania 16802*

**Michael J. Lercel and Harold G. Craighead***

*School of Engineering and Applied Physics and the National Nanofabrication Facility, Cornell University, Ithaca, New York 14853*

*Received: March 7, 1996; In Final Form: July 6, 1996*[⊗]

Highly organized monolayers formed from the self-assembly of octadecyl derivatives on oxide-covered Si and Ti substrates have been exposed to electron beam impact under typical conditions used in lithographic patterning. A combination of X-ray photoelectron spectroscopy, ellipsometry, infrared spectroscopy, and liquid drop contact angle measurements show that the major effect of irradiation is the loss of H, *via* cleavage of C−H bonds, to form a carbonaceous residue with a surface containing oxygenated functional groups.

## 1. Introduction

The formation of patterned, nanometer-scale structures has become a topic of intense interest recently because of the many possible scientific and technological applications of these structures.[1,2] For applications in microelectronic device fabrication, lithographic patterning at the nanometer-scale is most easily achieved using highly focused electron beams (e-beams).[3] However, as the device feature size diminishes below the submicrometer level, extreme demands are placed on the resolution capabilities of standard polymeric thin-film resist systems, and there is a need for development of new systems involving the smallest possible film thicknesses and intrinsic sizes of the molecular constituents.[4] In response to these requirements, self-assembled monolayers (SAMs), with thicknesses on the order of 1−3 nm and molecular diameters <1 nm,[5,6] have been considered as candidate systems, and recent work with *n*-octadecylsiloxane [ODS, $CH_3(CH_2)_{17}SiO_X$] and *n*-octadecanethiolate [ODT, $CH_3(CH_2)_{17}S-$] monolayers on GaAs and $SiO_2$, respectively, has demonstrated pattern transfer to these technologically important substrates.[7−12] These studies show that both positive and negative pattern formations are possible. For both systems, solution etching of the substrate occurs selectively in the irradiated regions while for the ODT/GaAs SAM, reactive ion etching (RIE) of the substrate occurs selectively in the nonirradiated regions. These examples clearly show that the functioning of these types of SAMs under various processing conditions depends critically upon the chemical and physical changes induced by e-beam irradiation, and thus a fundamental understanding of these latter processes is critical to improvements in efficiency. Previous studies of bulk-phase alkanes and polyolefins have shown that electron impact at a variety of kinetic energies generally cause C−H bond scission with production of transient free radicals.[13−15] However, because of the significant differences in the local molecular-scale environments between quasi-2-dimensional molecular films and 3-dimensional bulk materials, *e.g.*, with respect to energy accommodation, mass transport and interfacial effects, one cannot assume *a priori* that the detailed effects of e-beam impact on hydrocarbon type SAMs can be predicted accurately from these bulk studies. With this in mind, we have initiated studies of the effects of e-beam exposure on various types of SAM/substrate combinations. In this report we focus on the behavior of SAMs of ODS on oxide-covered Ti and Si substrates as a function of electron impact dose. The results show that, similar to bulk-phase irradiation in hydrocarbon materials, the major effect is the scission of C−H bonds leading to loss of hydrogen. However, a specific manifestation of these effects in the case of the thin-film structure of a SAM is the uniform compacting of the chains to form a reduced thickness, carbonaceous film whose surface properties are controlled by the presence of oxygenated functional groups at the ambient interface. It is these structural and chemical characteristics of the irradiated SAM which underlie both the selective permeability to solution-based substrate etchants and the selective resistance to RIE in lithographic applications.

## 2. Experimental Section

**2.1. Sample Preparation and Exposure.** The ODS SAMs were prepared on native-oxide covered Si and Ti substrates using octadecyltrichlorosilane (OTS; 95% purity, Aldrich Chemical Company, Inc., Milwaukee, WI) solutions. The silicon substrates consisted of double-side polished, infrared transparent single-crystal wafers of (111) orientation (Harrick Scientific, Ossining, NY) and were cleaned by an initial solvent degreasing (*e.g.*, $CHCl_3$) followed by immersion in hot peroxysulfuric acid solution and copious rinsing in ultrapure water.[16] The oxide layer was typically 20−35 Å in thickness. The Ti substrates were prepared by electron-beam evaporation onto silicon substrates and upon exposure to air formed a thin oxide overlayer, estimated to be ∼1 nm thick. Immediately before immersion into the OTS solutions, the surfaces of both types of substrates were cleaned by exposure in a UV−ozone chamber (Model UVC-100, Boekel Industries, Philadelphia, PA) for 30 min, hydrated by rinsing with ultrapure water (18 MΩ·cm, organic free *via* UV−ozone scrub), and then spin-dried. The SAMs were prepared with the reaction solutions maintained at a constant temperature of 20(±0.5) °C in an argon-purged glovebox, and the sample introduction and withdrawal were carried out under this atmosphere. The sources and handling of all reagents as well as the detailed preparation procedures have been described elsewhere.[16]

[†] Department of Chemistry.
[‡] Department of Materials Science.
[⊗] Abstract published in *Advance ACS Abstracts,* September 1, 1996.

S0022-3654(96)00705-8 CCC: $12.00 

Electron beam irradiation was carried out at selected doses in a vacuum chamber operating at a base pressure of $\sim 10^{-10}$ Torr. In our previous studies, fine-feature exposures were done on a JEOL JBX 5DIIU e-beam lithography system operating with a current density of 20 A/cm$^2$.[8] However, in order to allow characterization of the irradiated surfaces by standard techniques, it was necessary to change electron exposure tools since exposed areas of up to several cm$^2$ were required for the analyses. For this purpose, irradiation was carried out using a scanning Auger gun (Perkin-Elmer 590) operating at a beam current of ~500 nA and a corresponding current density of 65 A/cm$^2$. Since this current density is severalfold greater than that of the JEOL, differences in the details of the e-beam interactions, particularly localized heating and irradiation volume, were considered and shown to be negligible. First, simple estimates of the localized heating show increases of temperature to be within a few degrees. Second, differences in irradiated volume can be considered negligible on the basis of previous work by Kisza *et al*.[17] which shows that the radius of the backscattering circle in polymer films irradiated at different currents is roughly constant for a constant total dose.

**2.2. Monolayer Characterization.** The monolayer films were characterized before and after irradiation by single wavelength ellipsometry (SWE), liquid contact angle (LCA), and transmission and reflection infrared spectroscopy (TIRS and RIRS, respectively) measurements. In addition, X-ray photoelectron spectroscopy (XPS) and Auger electron spectroscopy (AES) analyses were performed on the irradiated samples.

The SWE measurements were carried out using a null ellipsometer (Rudolph AutoEL II, Rudolph Research, Fairfield, NJ) operating at 632.8 nm with a 70° angle of incidence and a beam size of ~2 mm. The ellipsometric angles were determined before the film preparation in order to determine the dielectric functions of the starting substrates. Since the substrates had varying thicknesses of native oxide, these dielectric functions are classified as pseudofunctions which are characteristic of the composite substrate structures. After film preparation, SWE measurements were taken again as well as after the subsequent e-beam exposures, and the corresponding film thicknesses were determined assuming a single, homogeneous, isotropic dielectric function for the film with the value approximated as $1.50 + 0i$. With this procedure, the unirradiated ODS film thicknesses were determined to be $26.4 \pm 1.0$ Å for both types of substrates. This value is in excellent agreement with the isotropic model value reported earlier for oxidized Si substrates.[16] The corresponding thicknesses of unirradiated ODT SAMs on GaAs were $15 \pm 2$ Å, in agreement with the earlier report.[18]

The LCA measurements were performed using the sessile drop mode in a controlled atmosphere chamber (Ramé−Hart Model 100 goniometer) filled with the vapor of the probe liquid. For all the SAMs, similar values of $\theta \simeq 114°$ and $\simeq 43°$ were obtained for the water and hexadecane contact angles. These values, reliable to within $\sim \pm 2°$, indicate that the SAMs possess surfaces densely covered by methyl groups.

The infrared spectra of ODS films on the $SiO_2$/Si substrates were obtained in the transmission mode (TIRS) using a Bomem MB-100 spectrometer equipped with a DTGS detector and operating at 4 cm$^{-1}$ resolution with an unpolarized beam at normal incidence to the sample. These spectra are reported as absorbance spectra, calculated as $-\log(I/I_O)$ where the $I_O$ spectrum is usually determined from a bare substrate wafer freshly cleaned by UV−ozone exposure. In order to minimize artifacts in $-\log(I/I_O)$ arising from the $I_O$ spectrum, the final $I_O$ spectrum was obtained by leaving the film sample of interest in place after the completion of the $I$ spectrum, exposing the sample directly to UV−ozone treatment using a dry air purge and 185 nm lamps (BHK, Inc., Pomona, CA) mounted adjacent to the sample surfaces in order to completely remove the film by oxidation. The primary advantage of this procedure is to avoid spectral artifacts arising from improper sample alignment, effects which can be significant for monolayer TIRS spectra. Spectra of the ODS/Ti SAMs were obtained in the reflection mode (RIRS) using a Biorad FTS-60 spectrometer interfaced with an in-house built external reflection optical system on a goniometer and equipped with a narrow band MCT detector. These spectra were obtained using p-polarized light incident at 86° and were collected at 2 cm$^{-1}$ resolution. The RIRS spectra are given as $-\log(R/R_O)$, where $R_O$ is the spectrum of a "bare" $TiO_2$/Ti substrate which had been freshly cleaned by UV−ozone exposure.

The spectra of the unirradiated ODS/Si are in excellent agreement with the previous reports[16,18] and indicate that the films were of high structural quality. The ODS/Ti RIRS spectra showed agreement of the C−H stretching mode peak positions with the ODS/Si SAMs, an indication that both ODS SAMs were of equally high structural integrity. The relative band intensities of the ODS spectra for the two substrates, however, were distinctly different but differed in a manner precisely expected on the basis of the differing intrinsic electromagnetic effects between the TIRS and RIRS modes.

The AES measurements were performed in sequence directly in the sample irradiation chamber. Typical parameters for obtaining the Auger spectra were 2 keV beam energy, 500 nA beam current, exposure area ~2 mm × 4 mm (although the edges are masked from the cylindrical mirror analyzer), electron multiplier voltages ~1450 V, and operating system pressures $\sim 5 \times 10^{-9}$ Torr. The XPS measurements of beam-damaged samples were performed in a Surface Science Laboratories SSL-100 X-ray photoelectron spectrometer with a monochromatic Al Kα source.

## 3. Results

**3.1. Compositional Changes by AES and XPS.** *3.1.1. Auger Electron Spectroscopy.* Since AES analyses were carried out *in situ* at base pressures of less than $4 \times 10^{-9}$ Torr, the presence of adventitious contamination on the freshly exposed surface was minimized. During the course of the irradiation, AES spectra in selected energy regions were collected by running short sets of scans using the electron energy analyzer. These intermittent spectra were then used to give elemental profiles as a function of the continuing e-beam exposure dose. However, since each AES spectral point takes a few seconds to accumulate, the earliest or "zero-point" spectrum which can be collected represents a finite dose on the sample, ~5−80 $\mu$C/cm$^2$ (depending on the analysis area). In order to quantify the dose−spectral intensity relationships, the Auger signal counts of a given peak, I, vs the input e-beam doses $d$, on the sample were fit to the convenient function[19]

$$I = I_O + (I_{SAT} - I_O)\tanh(d/c) \qquad (1)$$

The constant $I_O$ is the intensity from the initial or "zero" spectrum, $I_{SAT}$ is the intensity from the final or saturation dose spectrum, and c is an empirical factor chosen to make $\tanh(d/c) = 1.0$ at the saturation dose. The critical dose, $d_C$, defined as the value of $d$ at the midpoint intensity in the $I$ vs $d$ curve, $(I - I_O)/(I_{SAT} - I_O) = 0.5$, is calculated from the data as $d_C = c\tanh^{-1}(0.5)$. Figure 1 shows the C(KLL) and Ti(LMM) AES signals for increasing e-beam dose for an ODS/Ti film. A value of $d_C \simeq 350$ $\mu$C/cm$^2$ results from analysis of both curves. At high doses of ~2000 $\mu$C/cm$^2$, the decrease in the C(KLL) signal is ~9%. Similar decreases of ~12 and 15% are also seen for

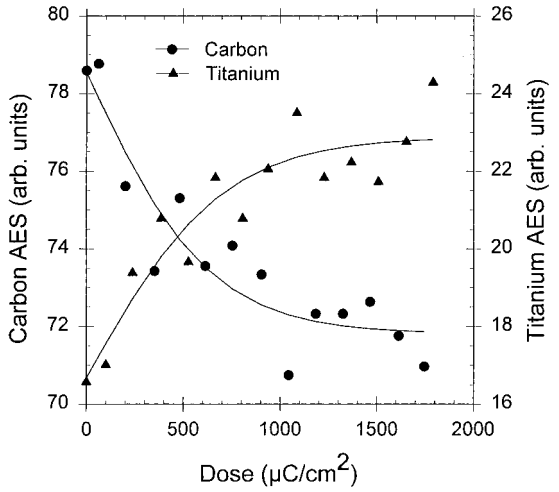


**Figure 1.** Auger electron signals for C(KLL) and Ti(LMM) vs electron beam dose for ODS/$TiO_2$/Ti. Auger spectra were obtained with 2 keV beam energy, ~450 nA beam current, and a 2 mm × 4 mm field of view for the e-beam exposure. The lines through the data points represent fits from eq 1 with line fit parameters of $I_O = 78.5$ $\mu$C/cm$^2$, $(I_{SAT} - I_O) = -6.72$ $\mu$C/cm$^2$ and $c = 635.27$ and a corresponding critical dose of ~350 $\mu$C/cm$^2$.

ODS/$SiO_2$ and ODT/GaAs films, respectively. Since the reproducibility of these signals is ~±4%, differences between the behaviors of the two SAMs may not be meaningful. Figure 1 also shows an ~40% increase in the Ti(LMM) signal at the high dose (~2000 $\mu$C/cm$^2$). These data were further analyzed by correcting the peak intensities for the effects of the Auger electron attenuation lengths $\lambda$ on the different depths of the target atoms. Using the general relation

$$\lambda = 9.0 + 0.022E \tag{2}$$

with $\lambda$ in Å and the Auger electron energy in eV, values of 14.75 and 18.12 Å were determined for the attenuation lengths of the C(KLL) and the Ti(LMM) electrons, respectively. In the absence of elastic scattering, the AES signal from the Ti substrate, $I_{Ti}$, when covered by a hydrocarbon layer of thickness $d$, is given by

$$I_{Ti} = I^{\infty}_{Ti} \exp[-d/\lambda_{OV}(E_{Ti}) \cos \theta] \tag{3}$$

where $\theta$ is the electron exit angle measured from the surface normal, with the specific value of 30° in this case, and $\lambda_{OV}$ is the electron escape depth in the overlayer medium, taken from eq 2.[20] The overlayer signal $I_{OV}$ is given by

$$I_{OV} = I^{\infty}_{OV}\left[\frac{1 + r_{Ti}}{1 + r_{OV}}\right][1 - \exp[-d/\lambda_{OV}(E_c) \cos \theta]] \tag{4}$$

where the $r$ values correspond to the backscattering terms for Ti and the overlayer, respectively. The backscattering terms are given by

$$r = (2.34-2.10Z^{0.14})U^{-0.35} + 2.58Z^{0.14}-2.98 \tag{5}$$

where $Z$ is the average atomic number of the matrix, taken as 2.64 for the SAM, and $U = E/E_C$ where $E$ is the incident electron energy, set to 2 keV, and $E_C$ is the energy of the C(KLL) electron.[20] The values of r were determined to be 0.5569 and −0.0566 for Ti and C, respectively. Using the above equations, the observed 40% increase in the Ti substrate signal (see above) at the highest dose corresponds to a decrease in the initial 26 Å SAM thickness by ~6 Å. This change, in turn, would result in an attenuation of the C signal by 8%, a value somewhat smaller than, but in good qualitative agreement with, the range of ~9−15% observed. The deviations could result from a number of factors, including the change in effective atomic number of the monolayer after irradiation, neglect of the effect of the interfacial siloxane layer, and the assumption that elastic scattering is absent.

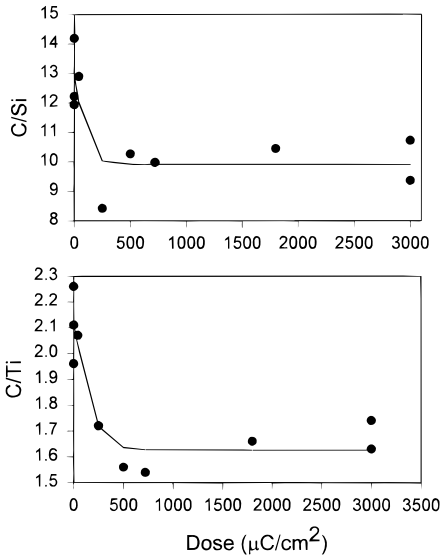


**Figure 2.** (C 1s)/(Ti 2p) and (C 1s)/(Si 2p) elemental ratios from XPS measurements on electron beam irradiated ODS/$TiO_2$/Ti films after exposure by 2 keV electrons.

*3.1.2. X-ray Photoelectron Spectroscopy.* The XPS spectra were first analyzed in terms of elemental ratios. The calculations were based on a sample structure involving an organic overlayer/siloxane (−$SiO_{1.5}$) underlayer configuration on both $SiO_2$/Si and $TiO_2$/Ti substrates, and the corrections for mean free path differences used the data of Laibinis *et al.*[21]

Figure 2 shows that the C(1s)/Si(2p) and C(1s)/Ti(2p) integrated peak intensity ratios decrease by ~25−30% with increasing irradiation. Fitting these data to eq 1 yields values of $d_C \simeq 120$ $\mu$C/cm$^2$. Above doses of ~500 $\mu$C/cm$^2$, further loss of the C(1s) intensity is negligible. The constant value of the Si/Ti peak intensity ratio demonstrates that the underlying siloxane layer remains intact during irradiation. These data show that the monolayer is only partially removed, in agreement with the AES data. After e-beam exposure, only slight increases of ~0.1 eV in the C(1s) line widths are observed. These data indicate little change in the binding energies (BEs) of the peaks and are consistent with the remaining carbon existing in the form of the original hydrocarbon chains (BE = 284.6 eV) and/or graphitic carbons (BE = 284.4 eV).[22] In addition, a low intensity high BE shoulder is seen, which upon simple deconvolution reveals the presence of three peaks at ~286.5, 288.0, and 289.5 eV. These can be ascribed, respectively, to the formation of groups containing −C−O− bonds (*e.g.*, alcohol, ether, ester, hydroperoxide), C═O (*e.g.*, aldehyde, ketone), and −$CO_2$− (carboxylic acid or ester).[23] Figure 3 shows the differences in the XPS spectra before and after irradiation. These higher BE carbon signals could arise from intrinsic changes in the irradiated film surface by subsequent reactions of transient radicals and reactive species in the irradiated film with $O_2$ and/or from deposition of atmospheric contaminants. However, copious rinsing using dichloromethane and ethanol immediately before introduction into the XPS chamber failed to remove these signals, an indication that they were not due to contamination. Further, carbon losses vs dosage trends are quite similar for the AES and XPS measurements. Since the AES spectra were conducted *in situ*, under vacuum conditions distinctly free of atmospheric contamination, this similarity strongly indicates that surface contamination is not a factor in the XPS measurements.

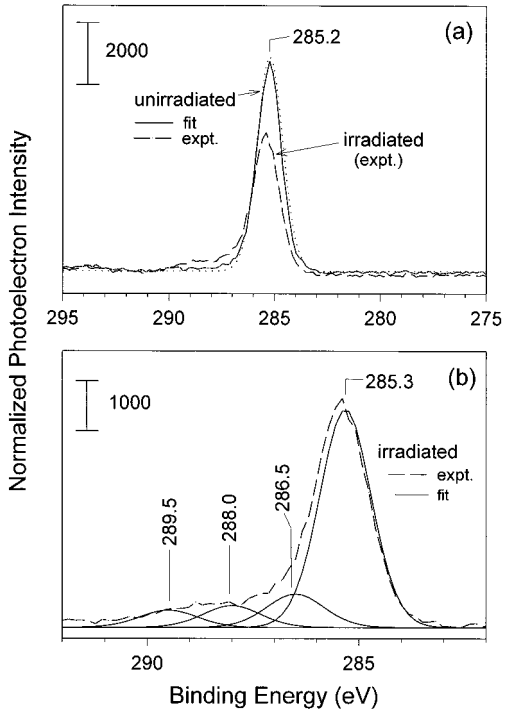


**Figure 3.** XPS C1s spectra of unirradiated and irradiated (∼1.8 mC/cm$^2$ dose of 2 keV electrons) regions of an ODS/Ti film. The photoelectron intensities for both spectra have been normalized to the respective Ti2p peak areas in order to adjust for differences in the absolute signal intensities for the two sets of spectra. Both sample regions were thoroughly rinsed in methylene chloride and ethanol after the electron beam exposure and before XPS analysis. Spectrum a shows the normalized experimental spectra for the unirradiated and irradiated (- - -) regions. Also shown is the single component fit (···) to the unirradiated spectrum with the fitted maximum at 285.2 eV. The diminished intensity of the irradiated region C 1s peak relative to the unirradiated region peak indicates a loss of C in the film after irradiation. Spectrum b shows the expanded normalized experimental spectrum of the irradiated region (- -) along with fitted component peaks (—) at 286.5, 288.0, and 289.5 eV which are assigned to −C−O, >C═O and −$CO_2$ groups.

Since the XPS analyses can involve up to several hours total X-ray irradiation of the samples, the possibility of X-ray-induced secondary electron damage to the SAM during the analysis was investigated. For this purpose, ODS films, some freshly made and some subsequently preexposed to e-beam dosing, were exposed to the monochromatized X-ray flux in the XPS chamber for extended times up to ∼6 h. Typical changes in the integrated C(1s) and Ti(2p) signals are given in Figure 4. It was observed that these types of changes are very dependent on the initial dosing conditions from the Auger beam. For example, after a 6 h. exposure to X-rays, at an anode power of 800 W, an initially unexposed ODS/Ti film shows an ∼8% loss in the C(1s) signal, with a corresponding increase in the Ti(2p) signal, while a film initially exposed at an ∼400 $\mu$C/cm$^2$ electron dose shows almost no change in either the C(1s) or the Ti(2p) signal after the X-ray irradiation. This comparison indicates that X-ray damage, primarily arising from the secondary electron emission in the sample,[24] induces the same fundamental types of changes in the film as the e-beam. However, e-beams are far more efficient in exposing the films as shown by the fact that ∼6 h. of X-ray exposure are required to produce the same damage as ∼1 min of e-beam exposure at 2 keV with a 500 nA beam current distributed over the field size of ∼8 mm$^2$.[25]

**3.2. Ellipsometric Thickness.** The SWE measurements indicate a decrease in the film thicknesses with increasing doses, as plotted in Figure 5. For ODS SAMs a limiting value of ∼16 Å is reached after a dose of ∼350 $\mu$C/cm$^2$. This thickness corresponds to an ∼35−42% loss of the SAM, quite similar to

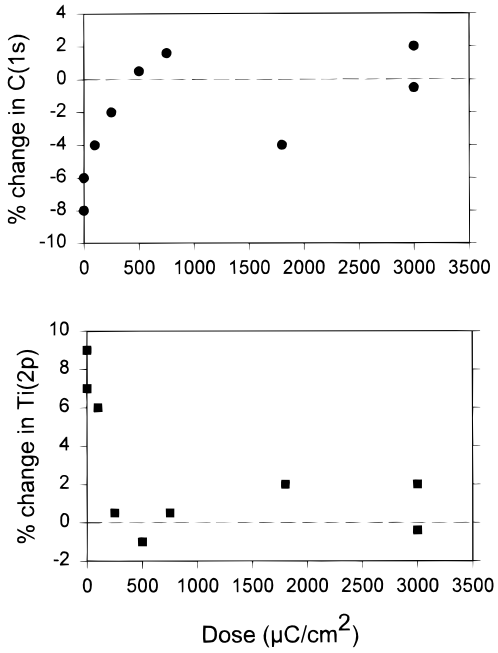


**Figure 4.** Changes in the C 1s and T 2p intensities with 6 h exposure to X-rays after irradiation with 2 keV electron beam at different doses. For comparison, the result of sample exposure to X-rays without any prior electron irradiation are the points corresponding to zero dose.

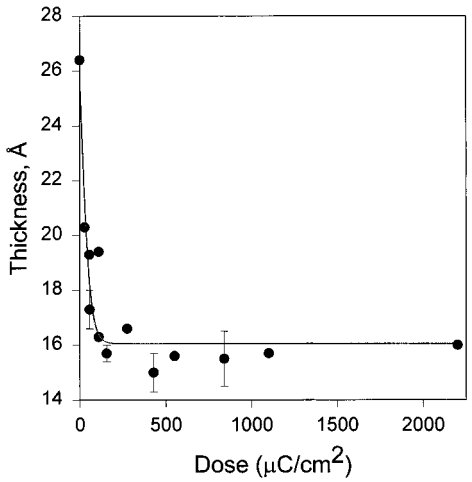


**Figure 5.** Thickness variations of an ODS/Si film as measured by ellipsometry after electron beam exposure at 2 keV. The thickness values were calculated assuming that the film optical constants were constant with those with values of $n = 1.50$ and $k = 0$. The curve was fit to eq 1, similar to that for the Auger spectra analyses, with fit parameters of $I_O = 25.99$ Å (initial film thickness in Å), $(I_O - I_{SAT}) = -9.93$ Å (change in film thickness at saturation dose) and $c = 55.27$, corresponding to a critical dose of ∼ 30 $\mu$C/cm$^2$.

the 25−30% losses derived from XPS measurements. In some cases the SWE measurements were carried out on samples that were previously subjected to the standard XPS analysis, and negligible differences were noted, in agreement with the earlier conclusion of minimal XPS sample damage. It is important to note that the values of the SAM optical constants assumed in the analysis of the ellipsometric data are not necessarily accurate for the e-beam-damaged films since the intrinsic electronic polarization response will be somewhat altered during irradiation. Unfortunately, the thicknesses of the damaged film are well below the limit for independent determination of the correct optical constants directly from the SWE data, i.e., the product of (refractive index) × (thickness) cannot be separated.[26] However, since one can reasonably expect that a carbonaceous film will exhibit somewhat higher values of the real refractive index than the original SAM, the values reported

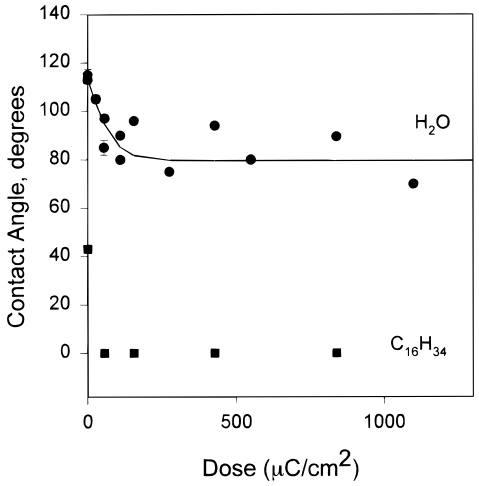


**Figure 6.** Contact angles of water and hexadecane ($C_{16}H_{32}$) on an ODS/$SiO_2$/Si film after electron beam exposure at 2 keV. Line a shows the fit to eq 1 with fit parameters of $I_O = 113.23$ (water contact angle for initial monolayer), $(I_O - I_{SAT}) = -33.6$ (change in contact angle at saturation dose) and $c = 91.4$ corresponding to a critical dose of ~50 $\mu$C/cm$^2$.

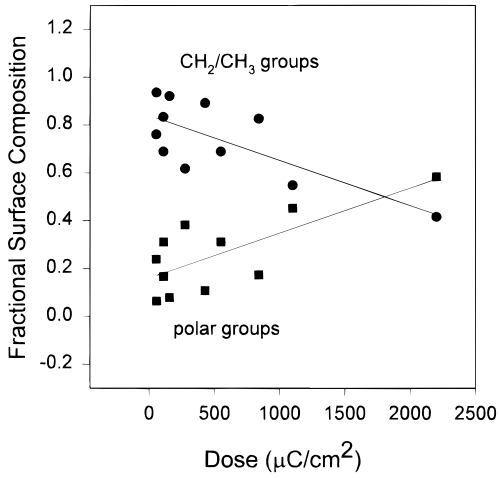


**Figure 7.** Estimation of the fractional surface composition from contact angle data using eq 6. The surface is assumed to consist entirely of $CH_3$, $CH_2$ and polar groups. For details see text.

here on the basis of the SAM refractive index will overestimate the actual thicknesses. Finally, we note that the ellipsometric data were quite constant at different points across the entire surface of any given sample as well as from sample to sample subjected to identical e-beam irradiation conditions. These observations indicate that the e-beam doses are uniform across the film surfaces.

**3.3. Liquid Drop Contact Angles.** The LCA measurements on the irradiated ODS/$SiO_2$ SAMs, summarized in Figure 6, show a sharp decrease in the water contact angles from 114° to ~80° upon irradiation. These data indicate corresponding distinct changes in the surface chemistry. Since it is generally agreed that the wetting responses of these organic films arise from the upper 0.5 nm surface regions,[27] a value slightly larger than the size of a $CH_3$ group, the wetting data then indicate that the irradiation changes the ambient interface from a layer of $CH_3$ groups to one also containing $CH_2$ and/or polar groups. The former are expected to be exposed at the surface when chain scission and/or chain disordering occur, and the latter could arise from reactions of reactive species formed during irradiation, such as primary carbon radicals, with oxygen upon exposure of the samples to air. A rough estimate of the fractional surface composition of the hydrophobic hydrocarbon groups, $CH_3$ and $CH_2$ combined, and the expected polar functional groups, such as OH and $CO_2H$, was made using standard wetting vs compositional relationships[28,29] applied to the water data. In particular we used the following relationship proposed by Israelachvili and Gee:

$$(1 + \cos\theta_c)^2 = f_1(1 + \cos\theta_1)^2 + f_2(1 + \cos\theta_2)^2 \quad (6)$$

In this equation, $\theta_c$ is the contact angle for the given probe liquid on a composite surface of microscopically heterogeneous patches, $f_1$ and $f_2$ represent the surface area fractions of the patches populated by groups 1 and 2, respectively, where $f_1 + f_2 = 1$, and $\theta_1$ and $\theta_2$ are the corresponding intrinsic contact angles of the probe liquid on these groups. The probe liquid in this case was taken to be water. The surfaces were assumed to be populated by a microscopic dispersion of hydrophobic $CH_3$ and $CH_2$ groups with $\theta \simeq 110°$ and polar groups (OH, $CO_2H$, etc) with $\theta = 0$. By incorporating the observed water contact angle data for the irradiated surfaces in eq 6, together with the constraint that $f_1 + f_2 = 1$, we determined the values of the fractional coverages of hydrophobic and hydrophilic groups, and the calculated surface chemical compositions are given in Figure 7 as a function of the e-beam dose. The observed decrease in the fraction of the combined hydrophobic $CH_2$ and $CH_3$ groups can be attributed to the loss of hydrogen atoms during the process.[30,31] Hexadecane contact angles were also measured for these surfaces, and in all cases e-beam irradiation results in a drop from the initial values of ~43° to nearly zero, equivalent to complete wetting. Since the initial surfaces exhibit a pure $CH_3$ character, while pure $CH_2$ surfaces, *e.g.*, polyethylene, are completely wetted by hexadecane, these data further show that e-beam irradiation causes a significant loss of $CH_3$ groups from the surface.

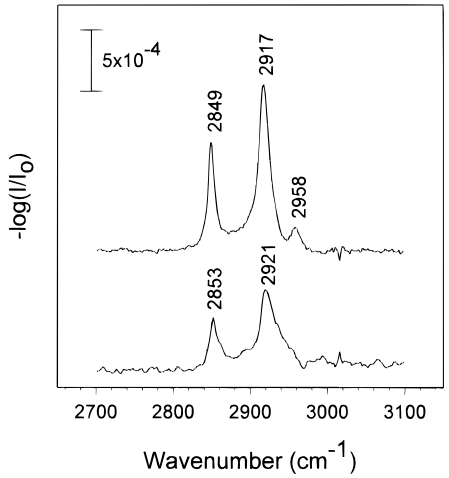


**Figure 8.** Change in the C−H stretching mode peaks of an ODS/$SiO_2$/Si sample upon irradiation with 2 keV electrons. The TIRS spectra were taken according to the *in situ* sacrificial procedure as described in the text which removes the unexposed ODS monolayer on the reverse side of the wafer. The lower spectrum corresponds to a single surface of ODS, and the upper spectrum corresponds to the irradiated surface alone. The spectrum of the irradiated sample is an average of several spectra taken with different samples irradiated with 2 keV beams with doses of 500 $\mu$C/cm$^2$.

**3.4. Infrared Spectroscopy.** The TIRS and RIRS measurements show strong changes in the high-frequency C−H stretching region upon irradiation. Figure 8 shows typical TIRS spectra of a ODS/$SiO_2$ SAM before e-beam exposure and after a dose of 500 $\mu$C/cm$^2$. The intensities of all the C−H mode peaks decrease significantly with increasing beam exposure as shown by the residual signal for the $CH_2$ symmetric and antisymmetric mode peaks at ~2850 and ~2920 cm$^{-1}$, respectively. Analysis of the integrated intensities of these peaks indicate a ~40% loss in the $CH_2$ C−H intensity which could be construed as roughly

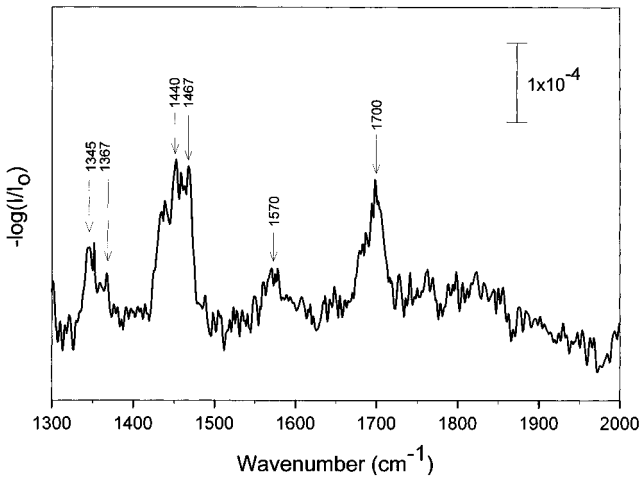


**Figure 9.** The low-frequency region of the same irradiated monolayer as used for the data in Figure 8. The only spectral feature of note for an unexposed ODS sample is the $CH_2$ deformation centered at 1467 $cm^{-1}$.

a 40% loss in the number of C−H bonds. Unfortunately, the signal/noise ratios preclude a similar analysis with the $CH_3$ peaks (C−H stretching modes). However, the observed vestige of the $CH_3$ antisymmetric mode peak, appearing as a high-frequency shoulder, indicates that not all methyl groups have been damaged and/or removed. Examination of the $CH_2$ peak frequencies shows that they shift upward from their original values in the unirradiated SAM by several $cm^{-1}$ while the peak widths increase by ∼50%. This observation indicates that the remaining $CH_2$ units of the irradiated SAM experience a significantly disordered environment. A typical damage product could be olefinic groups, but no significant peaks at the expected higher frequencies, which could indicate the presence of the C−H stretching modes of either vinylic or allylic groups, are observed. However, previous work has shown that these features are difficult to observe even in SAMs fully functionalized with unsaturated groups.[32]

The low-frequency spectrum shows multiple features that can be assigned to a number of groups present in the irradiated sample. Unfortunately, reliable data cannot be obtained below 1300 $cm^{-1}$ because of the spectral artifacts arising from reference spectra which do not precisely null the extremely strong bands of the Si−O phonon modes intrinsic to the Si substrates. The presence of polar groups, as indicated by XPS and LCA analyses, implies that oxygenated functional groups are present. On the basis of this assessment, the peaks observed at 1345 and 1570 $cm^{-1}$ were assigned to the symmetric and antisymmetric stretching modes of the carboxylate group ($CO_2^-$), respectively, while those at 1435 and 1700 $cm^{-1}$ can be assigned to the C−O and C═O vibrations in carboxylic acid groups, respectively. However, other oxygenated groups might well contribute, such as carbonyl groups from ketones, which could give rise to bands in the region 1705−1730 $cm^{-1}$. The peak at 1460 $cm^{-1}$ presumably has contributions from $CH_2$ deformations. Figure 9 summarizes these results. In order to confirm the assignment of the peaks at 1345 and 1570 $cm^{-1}$ to the $CO_2^-$ group, an attempt was made to convert such groups to the corresponding $CO_2H$ moieties by treating the surfaces with pH 2 hydrochloric acid solution. After the treated substrates were rinsed with water, the TIRS spectra of the samples were taken (data not shown) and these qualitatively show a partial disappearance of the 1345 and 1570 $cm^{-1}$ $CO_2^-$ peaks along with a corresponding increase in the ∼1700 $cm^{-1}$ $CO_2H$ peak. Upon subsequent treatment with pH 12 NaOH solution, the original spectrum is regenerated. This behavior lends strong support to the presence of $-CO_2H$ groups in the irradiated film. However, the fact that the alleged $CO_2^-$ peak did not completely disappear upon pH treatment suggests that a significant number of these groups are located in regions of the monolayer inaccessible to solution permeation.

**3.5. Microscopy: SEM and AFM.** *3.5.1. SEM.* Other indications of changes in surface structure and composition are seen by scanning electron microscopy (SEM) and atomic force microscopy (AFM). As has been observed by other groups,[33,34] we see a distinct darkening of SAM surfaces in the SEM after exposure to electron beams (data not shown). While one might speculate that this effect could be due to enhancement of adsorption of surface contamination as a result of increase in surface energy in the exposed regions, the Auger data taken at base pressures of $\sim 10^{-9}$ Torr also show surface changes, but the scan times here are less than those required for formation of a monolayer of contamination. This comparison suggests that the darkening effect in SEM is caused by differential secondary electron scattering or differential charging of the surface rather than preferential adsorption of contaminants.

*3.5.2. Corrections for Variations in Beam Energy.* The above surface analyses have been done on samples with large areas exposed at 2 keV with the scanning Auger gun. However, typically, and in our previous reports,[8,9,10,11] fine feature exposures are done at higher electron beam energies of around 50 keV. In order to compare the relative electron doses at these high-energy regimes with the present results at lower energies, one needs to account for the effects of beam energy on the electron dose. For this purpose, the actual energy deposited by the beams in the vicinity of the target atoms, buried at a distance $x$ from the sample surface, was calculated from the following modified Bethe continuous energy loss equation:[35]

$$(-\mathrm{d}E/\mathrm{d}x)_E = 785Z\rho \ln(1.166(E + kJ)/J)/(AE) \qquad (7)$$

where for a given medium, the quantities $(-\mathrm{d}E/\mathrm{d}x)_E$, $Z$, $\rho$, $J$, and $A$ are, respectively, the inherent electron stopping power or energy loss per unit length, the average atomic number, the density, the mean ionization energy, and the average atomic weight, while the quantity $E$ is the average electron energy across the electron trajectory. The quantity $k$ is a parameter whose value depends on the material under consideration and is used to correct the calculated stopping powers at lower incident beam energies obtained from the original Bethe stopping power equation.[36,37] Applying this equation to the same medium but for different average beam energies $E_1$ and $E_2$, we can calculate the ratios of the stopping powers at the two energies. For our calculations, the following values were assigned: $k \simeq 0.77$ (for carbon),[35] $Z = 2.64$ (average atomic number for $C_{18}H_{37}$), $A = 4.6$ (average atomic weight for $C_{18}H_{37}$), $\rho = 0.82$ g/cm$^3$, and $J \simeq 30.4$ eV ($J$ has been calculated from $J = 11.5$ for $Z < 13$). The quantity $E$ is the energy of the electrons in the material which can be assumed to be equal to the incident beam energy (a good approximation for the SAM thickness of ∼2.5 nm). With the above values for the input parameters, eq 7 leads to values of 0.48 and 0.069 for the ratios of the energies deposited in the SAM by the 5 and 50 keV beams, respectively, relative to a 2 keV beam. It follows that equivalent damage effects would be obtained with critical doses of ∼100 $\mu$C/cm$^2$ at 2 keV, ∼208 $\mu$C/cm$^2$ at 5 keV, and ∼1450 $\mu$C/cm$^2$ at 50 keV. Thus, the result is that at higher beam energies longer exposures are required.

*3.5.3. AFM.* In order to characterize the topographical changes induced in the films upon e-beam exposure, a few samples of ODS/$SiO_2$/Si were irradiated using a focused beam from a JEOL JBX 5DIIU electron beam lithography system. The topographies of the small irradiated areas were examined directly by AFM previously.[8] In the contact mode, the lateral

friction in the damaged regions causes apparent height variations much greater than the true height changes.[38] From the dependence of the AFM height on dose, a critical dose of ~160 $\mu$C/cm$^2$ at 50 keV was identified. When corrected using the modified Bethe equation (eq 7), the latter becomes equivalent to a critical dose of ~12 $\mu$C/cm$^2$ at 2 keV. In comparison, the experimental value derived from the analyses of the Auger-irradiated samples at 2 keV is about 160 $\mu$C/cm$^2$ . This indicates that there is a significant discrepancy between the critical doses as determined by AFM, which could be due to incorrect measurements in the heights of the features that have been measured. This is likely, as AES samples the bulk of the monolayer whereas AFM is more surface sampling in character.

Burnham *et al*.[38] have studied the effect of variations in the surface energy on the forces seen by the cantilever tip. For high surface energy samples such as graphite and mica, the tip jumps into contact with the sample once the gradient of the attractive force exceeds the cantilever spring constant. As the tip is withdrawn, there is a hysteresis due to the adhesive contact between the tip and the sample and this adhesive force is always greater than the attractive force. On the basis of this phenomenon, subtle changes in friction can be measured.

The lateral force on the AFM cantilever $F_{attr}$ can be determined from the difference in the apparent tip heights between forward and reverse scans, and the measurements give a value of ~60 nN. Assuming that only long range van der Waals forces are involved in the tip-surface interaction

$$F_{attr} = -4\pi R(\gamma_t\gamma_s)^{1/2} \tag{8}$$

where $R$ is the tip radius and $\gamma_t$ and $\gamma_s$ are the surface energies of the tip and sample. Estimating the values of $R$ and $\gamma_t$ as 30 nm and 300 mJ/m$^2$, respectively, and using the experimentally derived value of $F_{attr}$, $\gamma_s \simeq 85$ mJ/m$^2$. Since the actual value of $R$ is uncertain over the approximate range of 20−60 nm, $\gamma_s$ could range over 20−190 mJ/m$^2$. These numbers support our conclusions from the spectroscopic and wetting data that the irradiated surface has a considerably higher energy than does the original SAM and consists primarily of a graphitic residue together with some oxygenated groups.

**3.6. Chemical Reactivity.** The combination of the above characterization data shows that the irradiated SAM has lost a significant amount of the original aliphatic hydrocarbon character to become rather carbonaceous in character. On this basis, a few experiments were carried out to examine the changes in the general susceptibility of the irradiated layer toward aggressive chemical reagents which slowly attack the initial SAM. In these experiments, ODS/$SiO_2$/Si SAMs were irradiated at 500 $\mu$C/cm$^2$ and exposed to both strong solution- and gas-phase oxidants.

Immersion of the irradiated films in peroxysulfuric acid (4:1 $H_2SO_4$:$H_2O_2$) at 70 °C for varying times reveals selective attack. For exposures of about 1 min, the ellipsometric thicknesses drop by about half for the irradiated films while negligible change is seen for the original monolayer. In addition, the water contact angle also drops sharply for the irradiated film to ≤ 25° in 40 s indicating that a significant number of wettable groups are exposed along with material removal from the monolayer.

Similarly irradiated SAM samples were also exposed to ozone in a UV−ozone reactor for varying times, and the progress of the reactions was followed by SWE. It was observed that within the times generally required to remove nearly all of the irradiated film, no significant fraction of the original film was removed. The loss of the irradiated SAM is also accompanied by a continual lowering in the water contact angle.

## 4. Discussion

**4.1. Mechanistic Aspects.** Consistent with all the characterization data in this study, the salient features of the electron beam damage mechanism in hydrocarbon SAMs can be described in terms of well known electron impact and radical reactions for hydrocarbon irradiation.[13−15] For convenience of the discussion, these are summarized in eqs 9−17 as follows:

$$-CH_3 \xrightarrow{e^-} -CH_2^{\bullet} + H^{\bullet} \tag{9}$$

This sequence focuses only on the initial and main steps of

$$-CH_2- \xrightarrow{e^-} -CH^{\bullet}- + H^{\bullet} \tag{10}$$

$$-CH_2-CH_3 \xrightarrow{e^-} -CH_2^{\bullet} + CH_3^{\bullet} \tag{11}$$

$$-CH_2-CH_2- \xrightarrow{e^-} -CH_2^{\bullet} + {}^{\bullet}CH_2- \tag{12}$$

$$-CH_X^{\bullet} \xrightarrow{O_2} -CH_X-O-O^{\bullet} \tag{13}$$

$$-CH_X-O-O^{\bullet} \xrightarrow{[H^{\bullet}]} -CH_X-O-OH \tag{14}$$

$$-CH_X-O-OH \rightarrow >C{=}O,\ C-OH,\ -CO_2H,\ \textit{etc.} \tag{15}$$

$$-C^{(1)}H^{\bullet}- + -C^{(2)}H^{\bullet}- \xrightarrow{\text{cross-linking}} -C^{(1)}H_2-C^{(2)}H_2- \tag{16}$$

$$-(CH_2)_X- \xrightarrow{e^-} -C_YH_Z- \ (Y \simeq X,\ Z < 2X) \tag{17}$$

the highly complex sequences of free radical processes which can occur; many more reaction steps would need to be added in order to describe the complete sequence possible. The above reactions involve secondary electron-induced C−C and C−H bond scission (steps 9−12), reaction of transient radicals with $O_2$ to form hydroperoxide groups (step 13, occurring primarily upon removal from the exposure chamber), hydrogen radical abstraction and subsequent reaction and/or rearrangement to give oxygenated groups (steps 14 and 15), and interchain cross-linking *via* C-radical recombination (step 16). Step 17 describes the overall progress of the irradiation chemistry to give a preferential loss of H atoms, relative to C atoms, with eventual formation of a carbonaceous material. Because the films are of molecular thickness, it can be presumed that small, stable molecular species such as $H_2$, $CH_4$, $CH_3OH$, and $HCO_2H$ are completely lost to the atmosphere. Similarly, it is reasonable to assume that transport of $O_2$ into the film interior is extremely rapid relative to film handling times, and consequently, oxidative scavenging of the radical species within the film is effectively complete. This mechanism fully accounts for the following observed characteristics of the irradiated SAMs: loss of C atoms (AES and XPS), loss of C−H bonds (IRS), introduction of polar surface character (LCA), the presence of non-hydrocarbon C atoms (XPS) and $CO_2H$ groups (IRS), and increased surface energy (AFM).

The above mechanism is sufficiently general that it is essentially applicable to hydrocarbon materials ranging from bulk liquids and solids to molecular thickness films on solid substrates. In order to look for effects which may be specific to molecular films of the type used in the present study, the detailed results were compared with those from analogous studies of bulk materials.

A close parallel to the present study of $C_{18}H_{37}$-chain ODS SAMs is the electron irradiation study of *n*-octacosane, $C_{28}H_{58}$, by Miller *et al*. in which yields of fragment products up to $C_8H_{18}$

were reported.[39] In order to compare their results accurately with ours, it was necessary to correct their yield data to a per electron energy unit basis, *viz.*, the number of individual fragments produced per 100 eV of electron energy absorbed (the *G* value). These data were then used to predict the fragment pattern which might occur in the C18 SAM using the relationship $Y_X = E_{DEP}\, G_X$, where $Y_X$ is the yield of a fragment with the *G* value $G_X$ and $E_{DEP}$ is the total energy deposited by the electrons. The value of $E_{DEP}$ was determined from eq 7 for our conditions of a 2 keV beam, a dose of 500 $\mu$C/cm$^2$, and a SAM density of $4.5 \times 10^{14}$ chains/cm$^2$. After calculation of the values of $Y_X$ up to $X = C_8$ fragments, *viz.*, $H_2$ through $C_8H_{18}$, the predicted total H and C losses are ∼46 and ∼11%, respectively. These predictions appear to be in good agreement with the observed SAM changes: IRS, ∼40% loss of C−H bonds; AES, ∼30% loss of overlayer (from substrate signal changes); XPS, ∼25−30% loss of C; and SWE, ∼35−42% loss of film thickness. However, accurate direct comparisons are problematic. The only direct measure of the C loss is XPS which is higher than that predicted by roughly a factor of 2−3. The losses in the case of octacosane could be underestimated as "caging" of the carbon fragments can take place in the bulk whereas carbon fragments from the thinner monolayer can escape more efficiently. The other C-related numbers are more related to film thickness which is a function of film density and presumably the density increases on irradiation *via* cross-linking and partial carbonization. While the comparison of 46% H loss looks quite close to the ∼40% loss in C−H bond stretching intensity in the IRS, we note that the latter value must be corrected for contributions from unknown changes in the frequencies and cross sections of C−H bonds remaining incorporated within the disordered, carbonaceous product matrix.[40] In general, the agreement between the bulk and SAM irradiation experiments indicates that the overall electron impact mechanisms of the two material configurations are quite similar.

The observation of a significant presence of polar oxygen-containing moieties (*e.g.*, $CO_2H$) in the irradiated SAMs (IRS), particularly in the near surface regions (LCA), implies significant scavenging of transient radical species by $O_2$ (step 13) with reaction times less than those required for the sample analyses. Quantitative yield comparisons in terms of *G* values for bulk-phase and monolayer samples are not reasonable because of the significant differences in the magnitudes of the rates of oxygen diffusion to interior radical sites in the two cases. For example, it has been shown in the case of polyethylene that oxygen is soluble only in the amorphous regions of polyethylene.[41] Therefore, virtually no oxidation would be expected in the crystalline regions which have packing densities comparable to those in ODS SAMs. However, limited data are available which give *G* values of around 5.0 and 6.3 for the formation of C═O groups after oxygen exposure for several days, in linear and low density polyethylene, respectively.[42,43] This simple comparison underscores the intuitive conclusion that a major difference between bulk and monolayer film e-beam irradiation is the formation of a significant number of oxygenated functional groups in the monolayer films.

While it is clear that oxygen transport into the irradiated SAMs is capable of forming polar functional groups, a more subtle, but important issue for lithographic processing of the irradiated material is how these groups are distributed along the chains into the interior of the SAM. While the observed hexadecane contact angle data (Figure 6) show high losses of $CH_3$ character in the surface layer, the water contact angles indicate remnant hydrophobic character in the surface. Figure 7, based on water contact angle data, shows a residual 40% hydrophobic hydrocarbon character after the longest doses. These data suggest that a significant fraction of the oxygenated groups are located more than 0.5 nm deep (the wetting interaction range, see earlier) into the film interior. It has been shown that the free radicals produced in irradiated crystalline alkanes are located mostly at interior sites along the molecular chain; very few are at α-$CH_2$ sites and almost none at terminal positions.[44] Analogously, a significant fraction of radicals can be expected along the alkyl chains of the SAM, a situation which will lead to an appreciable number of buried oxygenated groups. In agreement with this expectation, only partial removal of the IRS peaks assigned to $CO_2H$ (at 1700 cm$^{-1}$ in Figure 9) could be effected by repeated treatment with pH 12 solution.

**TABLE 1: Summary of Critical Dose Values, All Corrected to 2 keV Impact Energies, Obtained from Different Sample Characteristics**

| | critical dose[a] from each type of analysis, $\mu$C/cm$^2$ | | | | | | |
|---|---|---|---|---|---|---|---|
| system | AES | XPS | wetting | ellipsometry | AFM | wet etch[b] | dry (plasma) etch[c] |
| ODS/$TiO_2$/Ti | ∼350 | 130, 110 | ∼50 | ∼30 | | | |
| ODS/$SiO_2$/Si | ∼350 | | ∼50 | ∼30 | ∼52[d] | ∼12[e] | |
| ODT/GaAs | ∼350 | | | | 12 | ∼7 | ∼350 |

[a] All values are compared on the common basis of a 2 keV electron impact energy. Corrections of the experimental data taken at different electron energies were made using the modified Bethe equation (eq 7) as described in the text. [b] Critical dose defined in terms of the threshold for formation of a positive contrast pattern by HF etching of the substrate in the irradiated region. Data taken from previous work [see ref 9]. [c] Critical dose defined in terms of the threshold for formation of a negative contrast pattern by RIE. Data taken from previous work [see ref 11] where a critical dose of ∼700 $\mu$C/cm$^2$ was observed at a 5 keV beam energy. [d] Corresponds to 31 $\mu$C/cm$^2$ at 1 keV. [e] Corresponds to 160 $\mu$C/cm$^2$ at 50 keV.

**4.2. Lithographic Aspects.** One of the driving forces for carrying out the present study was the need to provide a fundamental understanding of the microscopic basis for the ability of e-beam-irradiated SAMs to perform as ultrahigh resolution resists for substrate patterning. The present data show that the irradiated regions of SAMs are converted to a stable, carbonaceous film with a polar, somewhat water wettable surface. It is the properties of this residual film which then dictate the contrasts which are possible in subsequent pattern formation. Each of the different characteristics which were investigated in this study exhibit different critical doses above which the characteristic changes strongly. However, it is clear that these doses fall into two regimes of values, as indicated in the summary given in Table 1: 12−52 $\mu$C/cm$^2$ for onset of thickness shrinkage (ellipsometry and AFM) and surface wettability and 120−350 $\mu$C/cm$^2$ for onset of significant material (C atoms) loss (XPS and AES). One also can note in Table 1 that the critical doses associated with the onset of pattern transfer by wet etching (positive contrast) and dry etching (RIE, negative contrast), respectively, fall into these same two regimes of values.

In the case of positive pattern formation on $SiO_2$/Si, $TiO_2$/Ti and GaAs,[9−11] it has been observed that aqueous etch solutions show high selectivity for etching through the irradiated regions relative to the unirradiated SAM. Two factors would appear responsible for this. The correlations of critical dose values in Table 1 suggest that the critical factors in determining the onset of wet etch pattern transfer is the formation of polar surface groups and the film shrinkage. These can be understood straightforwardly in terms of an etching mechanism in which (1) the appearance of polar groups lowers the energy of the etch solution/substrate interface, relative to that for the nonirradiated case, and leads to more uniform contact with the etchant and (2) the dimensional changes in the irradiated film produce

a variety of nanometer-scale defects (microcracks) which leads to enhanced transport of the etchant to the substrate. The latter aspect is supported by the observed increase in molecular disorder shown by the IRS data. The onset of both of these factors occurs at low critical doses and can be associated with the processes of C−H bond cleavage, shown in eqs 9 and 10, and the subsequent oxygenation of residual radicals *via* eq 13.

In other studies we have observed that negative contrast patterns can be obtained by the use of RIE processes, *e.g.*, using low-energy $Cl^-$ ion plasmas on ODT/GaAs SAMs.[11] These observations indicate that the irradiated SAM regions are relatively inert to plasma etching, relative to unexposed regions. The ODT/GaAs example above was for the case of a $Cl^-$ RIE etch where a critical dose of 350 $\mu C/cm^2$ was reported. The correlation between this high critical dose and the similar values given in Table 1 for the onset of massive film degradation *via* C loss suggests that the critical factor involved in this plasma etch resistance is the appearance of the highly H-deficient, carbonaceous character of the film.[45] The IRS data show that at quite low doses substantial H loss occurs to (eqs 9 and 10) to provide a C-rich film. At much increased doses, the XPS and AES data show that the degradation of this carbonaceous film begins with the loss of C-containing fragments. The latter also implies that the onset of extensive film cross-linking (eq 16) begins at these high doses. It is known that cross-linked carbon exhibits a low sputter yield[46] and that this property correlates with the high sublimation energy of carbon.[47] On this basis one could expect that cross-linking of the damaged chains in the film will lead to a lower sputter yield and also that the products formed by reaction with the attacking $Cl^-$ ions will have a lower volatility.

The above comparisons show that there are fundamental differences in the required characteristics of the irradiated monolayer films for achieving optimum pattern contrast by solution- and reactive gas-phase ion etching processes. These conclusions, based on two specific types of processes, underscores the need to fully characterize the microscopic details of the irradiation mechanism in order to efficiently design high-contrast lithographic processes.

**Acknowledgment.** This work has been supported by grants from the Advanced Research Projects Agency, under the ULTRA initiative and the National Science Foundation (Grant DMR-900-1270, REU for K.F.).

## References and Notes

(1) Mallon, J. In *Nanotechnology*; Crandall, B. C.; Lewis, J., Eds.; The MIT Press: Cambridge, 1992; pp 215−239.

(2) Drexler, K. E.; Peterson, C. *Unbounding the Future: The Nanotechnology Revolution*; William Morrow and Co., Inc.: New York, 1991.

(3) Gentili, M.; Giovanella, C.; Selci, S. *Nanolithography: A Borderland between STM, EB, IB and X-Ray Lithographies*; Kluwer Academic Publishers: Dordrecht, The Netherlands, 1994.

(4) Chang, T. H. P.; Muray, L. P.; Staufer, U.; McCord, M. A.; Kern, D. P. In *Technology of Proximal Probe Lithography*; Marrian, C. R. K., Ed.; SPIE Optical Engineering Press: Bellingham, WA, 1993; pp 127−154.

(5) Ulman, A. *Introduction to Ultrathin Organic Films: from Langmuir-Blodgett to Self-Assembly*; Academic: San Diego, CA, 1991.

(6) Ulman, A. *Chem. Rev.* **1996**, *96*, 1533−1554.

(7) Tiberio, R. C.; Craighead, H. G.; Lercel, M. J.; Lau, T.; Sheen, C. W.; Allara, D. L. *Appl. Phys. Lett.* **1993**, *62*, 476.

(8) Lercel, M. J.; Tiberio, R. C.; Chapman, P. F.; Craighead, H. G.; Sheen, C. W.; Parikh, A. N.; Allara, D. L. *J. Vac. Sci. Technol.* **1993**, *B11*, 2823−2828.

(9) Lercel, M. J.; Redinbo, G. F.; Pardo, F. D.; Rooks, M.; Tiberio, R. C.; Simpson, P.; Craighead, H. G.; Sheen, C. W.; Parikh, A. N.; Allara, D. L. *J. Vac. Sci. Technol.* **1994**, *B12*, 3663−3667.

(10) Lercel, M. J.; Redinbo, G. F.; Rooks, M.; Tiberio, R. C.; Craighead, H. G.; Sheen, C. W.; Allara, D. L. *Microelectron. Eng.* **1995**, *27*, 43−46.

(11) Lercel, M. J.; Rooks, M.; Tiberio, R. C.; Craighead, H. G.; Sheen, C. W.; Parikh, A. N.; Allara, D. L. *J. Vac. Sci. Technol.* **1995**, *B13*, 1139−1143.

(12) Lercel, M. J.; Craighead, H. G.; Parikh, A. N.; Seshadri, K.; Allara, D. L. *Appl. Phys. Lett.* **1996**, *68*, 1504−6.

(13) Salovey, R. In *The Radiation Chemistry of Macromolecules*; Dole, M., Ed.; Academic Press: New York, 1973; pp 307−312.

(14) Chappas, W. J.; Silverman, J. *Radiat. Phys. Chem.* **1980**, *16*, 437−443.

(15) Földiák, G. *Radiation Chemistry of Hydrocarbons*; Elsevier Scientific Publishing Company: Amsterdam, 1981.

(16) Parikh, A. N.; Allara, D. L.; Azouz, I. B.; Rondelez, F. *J. Phys. Chem.* **1994**, *98*, 7577−7590.

(17) Kisza, M.; Maternia, Z.; Radzimski, Z. *J. Phys. D: Appl. Phys.* **1981**, *14*, 907−912.

(18) Sheen, C. W.; Shi, J.; Parikh, A. N.; Martensson, J.; Allara, D. L. *J. Am. Chem. Soc.* **1992**, *114*, 1514.

(19) The data also can be fit reasonably well by a first-order exponential decay function such as:

$$I = (I_O - I_{SAT}) \exp(-kd) + I_{SAT}$$

This equation and eq 1 give nearly identical values for the critical dose. However, since the specific kinetic rate laws describing the critical dose behavior are expected to be quite complicated because of the multiple contributing processes and the complexities of the solid state matrix, no attempt was made to determine a fundamental rate law. On this basis, the tanh function, which contains multiple exponential terms, was chosen for the fitting.

(20) Seah, M. P. In *Practical Surface Analysis*; Briggs, D., Seah, M. P., Eds.; John Wiley & Sons: Chichester, England, 1990; Vol. 1, (Auger and X-ray Photoelectron Spectroscopy); Chapter 5.

(21) Laibinis, P. E.; Bain, C. D.; Whitesides, G. M. *J. Phys. Chem.* **1991**, *95*, 7017−7021.

(22) Moulder, J. F.; Stickle, W. F.; Sobol, P. E.; Bomben, K. D.*Handbook of X-ray Photoelectron Spectroscopy*; Perkin Elmer: Eden Prarie, MN, 1992.

(23) Briggs, D. In *Practical Surface Analysis*; Briggs, D., Seah, M. P., Eds.; John Wiley & Sons: Chichester, England, 1990; Vol. 1, (Auger and X-ray Photoelectron Spectroscopy); Chapter 9, pp 469.

(24) A detailed investigation has been conducted on the role of X-rays in damage to trifluoroacetamide-terminated monolayers on different substrates, and the results are consistent with the premise that electrons scattered from the film are responsible for damage rather than the X-rays. Differences in the loss of fluorine atoms correlates with the efficiency of secondary electron generation from a given substrate. See: Graham, R. L.; Bain, C. D.; Biebuyck, H. A.; Laibinis, P. E.; Whitesides, G. M. *J. Phys. Chem.* **1993**, *97*, 9456−9464.

(25) In order to interpret these results on the two substrates in a quantitative way, it is necessary to consider the effects of low-energy secondary electrons emitted from the substrate since their yield, in principle, will be dependent on the specific electronic properties of each type of substrate. However, in the present case, these effects would appear to be small since the secondary electron yields as well as energy distributions from both $SiO_2$ as well as $TiO_2$ are similar, peaking at about 9−15 eV. The closest reported study to the present work appears to be that of Hayes and Evans (Hayes T. R; Evans, J. F. *Surf. Sci.* **1985**, *159*, 466−484), in which differences observed in the electron-stimulated desorption yields of adsorbed trimethylsilyl groups on $SiO_2$ and $TiO_2$ surfaces were attributed to the differing band structures of the two substrates and the relative positions of the adsorbed species' ionization potentials. In brief, electron impact first causes bonds to fragment to radicals, a process which, according to our above conclusion based on electron yields and distributions, should not exhibit much substrate dependence. However, the desorption yields will be strongly affected by the ability of the substrate valence band electrons to neutralize any ions formed in the initial process. In the present case of irradiation of a cross-linked SAM, since for both substrates a very similar nonvolatile carbonaceous residue is the primary product with desorption a minor product channel, the substrate-dependent neutralization efficiency should not be a controlling factor.

(26) Collins, R. W.; Kim, Y. T.; Shi, J.; Allara, D. L. In *Characterization of Organic Thin Films*; Ulman, A., Ed.; Manning: Greenwich, CT, 1995; pp 33−55.

(27) Atre, S. V.; Liedberg, B.; Allara, D. L. *Langmuir* **1995**, *11*, 3882−3893.

(28) Cassie, A. B. D.; Baxter, S. *Trans. Faraday Soc.* **1944**, *40*, 546.

(29) Israelachvili, J. N.; Gee, M. L. *Langmuir* **1988**, *5*, 288−289.

(30) Baer, D. R.; Engelhard, M. H.; Schulte, D. W.; Guenther, D. E.; Wang, L.-Q.; Rieke, P. C. *J. Vac. Sci. Technol.* **1994**, *A12*, 2478−2485.

(31) Rowntree, P.; Dugal, P.-C.; Hunting, D.; Sanche, L. *J. Phys. Chem.* **1996**, *100*, 4546−4550.

(32) Allara, D. L.; Nuzzo, R. G. *Langmuir* **1985**, *1*, 52.

(33) López, G. P.; Biebuyck, H. A.; Whitesides, G. M. *Langmuir* **1993**, *9*, 1513−1516.
(34) Wollman, E. W.; Frisbie, C. D.; Wrighton, M. S. *Langmuir* **1993**, *9*, 1517−1520.
(35) Joy, D. C.; Luo, S. *Scanning* **1989**, *11*, 176.
(36) Bethe, H. *Ann. Phys.* **1930**, *5*, 325.
(37) Bethe, H.; Ashkin, J. In *Experimental Nuclear Physics*; Segrè, E. Ed.; Wiley: New York, 1953; p 252.
(38) Burnham, N. A.; Dominguez, D. D.; Mowery, R. L.; Colton, R. J. *Phys. Rev. Lett.* **1990**, *64*, 1931−1934.
(39) Miller, A. A.; Lawton, E. J.; Balwit, J. S. *J. Phys. Chem.* **1956**, *60*, 599.
(40) Experiments are in progress using forward recoil elastic scattering (FRES) analysis to determine the H atom content in these films.
(41) Michaels, A. S.; Bixler, H. J. *J. Polym. Sci.* **1961**, *50*, 393.
(42) Matsuo, H.; Dole, M. *J. Phys. Chem.* **1959**, *63*, 837.
(43) Giberson, R. C. *J. Phys. Chem.* **1962**, *66*, 463.
(44) Kimura, K.; Ogawa, M.; Matsoi, M.; Karasawa, K.; Imamura, M.; Tabata, Y.; Oshima, K. *J. Chem. Phys.* **1975**, *63*, 1797.
(45) However, we note that this comparison must be taken in a very qualitative way since the electron beam damage process could vary between substrates due to differences in the secondary electron processes associated with the substrate. In general, we expect these differences to be small as judged from the limited amount of damage characterization data for ODT/GaAs samples which show that properties, *e.g.*, wetting, are quite similar in terms of dose dependence to the present ODS/$SiO_2$/Si and $TiO_2$/Ti cases. See also footnote 25.
(46) Matsunami, N.; Yamamura, Y.; Itikawa, Y.; Itoh, N.; Kazumata, Y.; Miyagawa, S.; Morita, K.; Shimizu, R.; Tawara, H. *At. Data Nucl. Data Tables* **1984**, *31*, 1.
(47) Kittel, C. *Introduction to Solid State Physics*; John Wiley and Sons: New York, 1986; p 55.

JP960705G